Production of sneutrinos in e^+e^- annihilation with polarized beams

M. Wendel and H. Fraas
Physikalisches Institut, Universität Würzburg, D-8700 Würzburg, Federal Republic of Germany
(Received 26 December 1990)

We study the production of sneutrinos in e^+e^- annihilation with polarized beams. Differential and total cross sections as well as their polarization asymmetries are given in general and in four representative chargino mixing scenarios for the case of a light and a heavy sneutrino.

I. INTRODUCTION

Although recent experiments in the Z^0 region [1] at the CERN e^+e^- collider LEP have given no evidence for the existence of supersymmetric partners of the standard particles, the idea of supersymmetry has not yet lost its attractiveness. Thus the search for supersymmetric particles will certainly be one of the main goals in exploring the energy range up to 200 GeV center-of-mass energy accessible to future phases of LEP and other accelerators.

The process $e^+ + e^- \to \tilde{\nu} + \bar{\tilde{\nu}}$, where $\tilde{\nu}$ is the scalar supersymmetric partner of the electron, muon, or τ neutrino, respectively, has been extensively discussed by Chiappetta *et al.* [2]. It is especially the production of $\tilde{\nu}_e$ proceeding via Z^0 exchange in the s channel and exchange of charginos $\tilde{\chi}_k^+$ $(k=1,2)$ in the t channel (see Fig. 1) which shows several interesting features. Owing to the chiral structure of chargino couplings, a strong dependence on the beam polarization is to be expected.

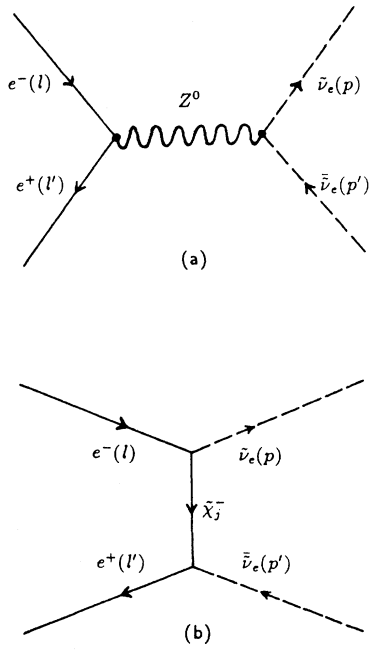

FIG. 1. Feynman graphs for $e^+ + e^- \to \tilde{\nu}_e + \bar{\tilde{\nu}}_e$. In the case of $\tilde{\nu}_{\mu,\tau}$ production, only Z^0 exchange contributes to the process.

Since the chargino couplings are a function of W-ino–charged-Higgsino mixing, we also expect strong variations of cross sections and polarization asymmetries with mixing scenarios at high energies, i.e., in some distance from the Z^0 peak. Moreover, polarization is interesting because of the change of sign of some spin asymmetries when going from SUSY-particle production to the production of standard particles [2].

These observations, together with the confidence that highly polarized beams can be obtained at LEP [3], motivate the examination of sneutrino pair production with polarized particle beams, particularly taking into account the mixing properties of charginos. For $\tilde{\nu}_\mu$ and $\tilde{\nu}_\tau$, the reaction only proceeds via Z^0 formation in the s channel. Therefore at energies far enough beyond the Z^0 peak, $\tilde{\nu}_e$ production, on the one hand, and $\tilde{\nu}_\mu$ or $\tilde{\nu}_\tau$ production, on the other hand, should display a rather different behavior.

Clearly, for detecting sneutrinos, reasonable decay rates into channels with characteristic signatures are as crucial as sufficient production rates. If the $\tilde{\nu}$ is heavy enough, observable decay modes with an interesting ex-

TABLE I. Chargino mass eigenvalues and mixing parameters in four different mixing scenarios. Shown are the mass eigenvalues m_i and their signs η_i $(i=1,2)$ as well as the mixing parameters of the charginos $V_{11}=-V_{22}=\cos\phi_+$, $V_{12}=V_{21}=\sin\phi_+$ used in Eqs. (2.3) and (2.6). M,μ, and $\tan\beta=\cot\theta_v$ are the parameters of the charged-gaugino–Higgsino mass matrix (see Refs. [6] and [7] for details).

	Scenarios of chargino mixing			
Parameter	A	B	C	D
M (GeV)	−36.4	+160.3	−22.8	+182.2
μ (GeV)	+72.9	+151.2	+100.2	+100.2
$\tan\beta=\cot\theta_v$	1.23	1.23	1.73	1.73
m_2 (GeV)	76.4	76.4	54.8	55.3
η_2	+1	−1	+1	−1
m_1 (GeV)	116.5	235.6	142.6	230.1
η_1	+1	+1	+1	+1
$V_{11}=-V_{22}$	0.266	0.708	0.202	0.817
$V_{21}=+V_{12}$	0.964	0.706	0.979	0.576

perimental signature would be three- or four-body decays (see [2], [4], and [5], for instance) with several leptons and/or jets in the final state. Since, however, the branching ratios of these decay modes are sensitively dependent on the masses and the nature of the charginos and also of the neutralinos, we have refrained from a discussion of sneutrino decay and shall only give results for their production.

In Sec. II we shall present formulas for differential and total cross sections as well as polarization asymmetries with general chargino mixing. Section III contains numerical results and a discussion for four representative scenarios of chargino mixing, as well as for different sneutrino masses. In an appendix we shall briefly summarize some notations and conventions used for the description of beam polarization.

The Lagrangian underlying our analysis is that of the minimal supersymmetric extension of the standard model, described in detail, for instance, in Ref. [6].

II. CROSS SECTIONS AND ASYMMETRIES

The Feynman graphs contributing to the process $e^+ + e^- \to \tilde{\nu}_e + \bar{\tilde{\nu}}_e$ are shown in Fig. 1. Denoting the four-momenta of $e^-, e^+, \tilde{\nu}_e$, and $\bar{\tilde{\nu}}_e$ with l, l', p, and p', respectively, we introduce the variables $s=(l+l')^2, t=(l-p)^2$, and $u=(l-p')^2$. The relevant couplings of the supersymmetric particles can be deduced from the following interaction Lagrangians of the minimal supersymmetric extension of the standard model (as for notations and conventions, we closely follow [6]):

$$\mathcal{L}_{\tilde{\nu}\bar{\tilde{\nu}}Z} = \frac{-ig}{2\cos\theta_W} Z_\mu \tilde{\nu}_e^* \overleftrightarrow{\partial}^\mu \tilde{\nu}_e \ , \tag{2.1}$$

$$\mathcal{L}_{e\tilde{\nu}\tilde{\chi}} = -g[(V_{11}^* \bar{\tilde{\chi}}_1^{+c} + V_{21}^* \bar{\tilde{\chi}}_2^{+c}) P_L e \tilde{\nu}_e^*] - g[\bar{e} P_R (V_{11} \tilde{\chi}_1^{+c} + V_{21} \tilde{\chi}_2^{+c}) \tilde{\nu}_e] \ . \tag{2.2}$$

In Eq. (2.2), $\tilde{\chi}_i^+$ $(i=1,2)$ and e are four-component spinors, while $\tilde{\nu}_e$ is the field of the sneutrino. $\tilde{\chi}_i^{+c}$ are charge-conjugated spinor fields. Furthermore, $P_{R,L}=(1\pm\gamma_5)/2$ denote the right- and left-handed projection operators, $g=e/\sin\theta_W$ $(e>0)$ and V_{kl} is the 2×2 unitary matrix appearing in the diagonalization of the W-ino–charged-Higgsino mass matrix ($V_{11}=-V_{22}=\cos\phi_+$, $V_{12}=V_{21}=\sin\phi_+$, see [7] for more details).

Owing to the chiral structure of the couplings, there is a strong dependence of the *chargino exchange* on the beam polarizations. The only nonvanishing helicity amplitude for this partial process is

$$F_{-1/2+1/2}(\tilde{\chi}) = \frac{ie^2 E}{m_e \sin^2\theta_W} p \sin\theta \, e^{-i\varphi} \times \sum_{j=1,2} |V_{j1}|^2 D_j(t) \ , \tag{2.3}$$

where $D_j(t)=(t-m_j^2)^{-1}$, m_j being the (positive-valued) mass of the chargino ($m_1 > m_2$ in our notation). $\lambda=-\frac{1}{2}$ and $\lambda'=+\frac{1}{2}$ are the helicities of the electron and the positron, respectively. $E=\frac{1}{2}\sqrt{s}$ is the beam energy and p denotes the (absolute value of) the $\tilde{\nu}_e$ momentum in the e^+e^- center-of-mass system. The angles θ and φ are determined by the direction in which the $\tilde{\nu}_e$ is observed:

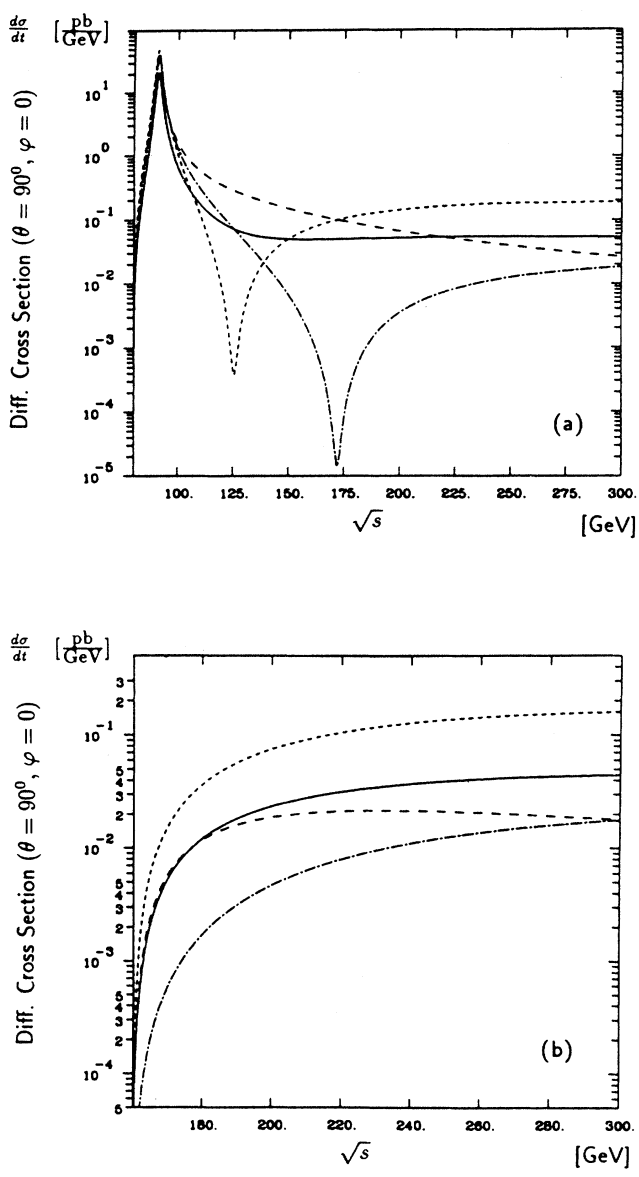

FIG. 2. Energy dependence of the differential cross section of $e^-e^+ \to \tilde{\nu}_e \bar{\tilde{\nu}}_e$ ($\theta=90°$, $\varphi=0$, scenario D) for different beam polarizations. (a) for $M_{\tilde{\nu}_e}=40$ GeV, (b) for $M_{\tilde{\nu}_e}=80$ GeV. Solid line denotes unpolarized, short-dashed line denotes long_{-+}, long-dashed line denotes long_{+-}, and dashed-dotted line denotes transverse.

θ is the "scattering angle" between **p** and l (l being identical with the z axis), while φ is meaningful only in polarized configurations and measures the angle between **p** and the x axis (see the Appendix for more information).

For Z^0 *exchange,* the nonvanishing helicity amplitudes are

$$F_{+1/2-1/2}(Z^0)=\frac{ie^2E}{m_e c_W^2}p\sin\theta\, e^{i\varphi}D_z(s)\ , \tag{2.4}$$

$$F_{-1/2+1/2}(Z^0)=\frac{ie^2E(c_W^2-s_W^2)}{m_e s_W^2 c_W^2}p\sin\theta\, e^{-i\varphi}D_z(s)\ . \tag{2.5}$$

where now $D_z(s)=(s-m_z^2+im_z\Gamma_z)^{-1}$ and $s_W=\sin\theta_W$, $c_W=\cos\theta_W$. Equations (A5) and (A6) given in the Appendix together with the appropriate flux and normalization factors yield the differential cross section for the production of *electron sneutrinos* for general beam polarization:

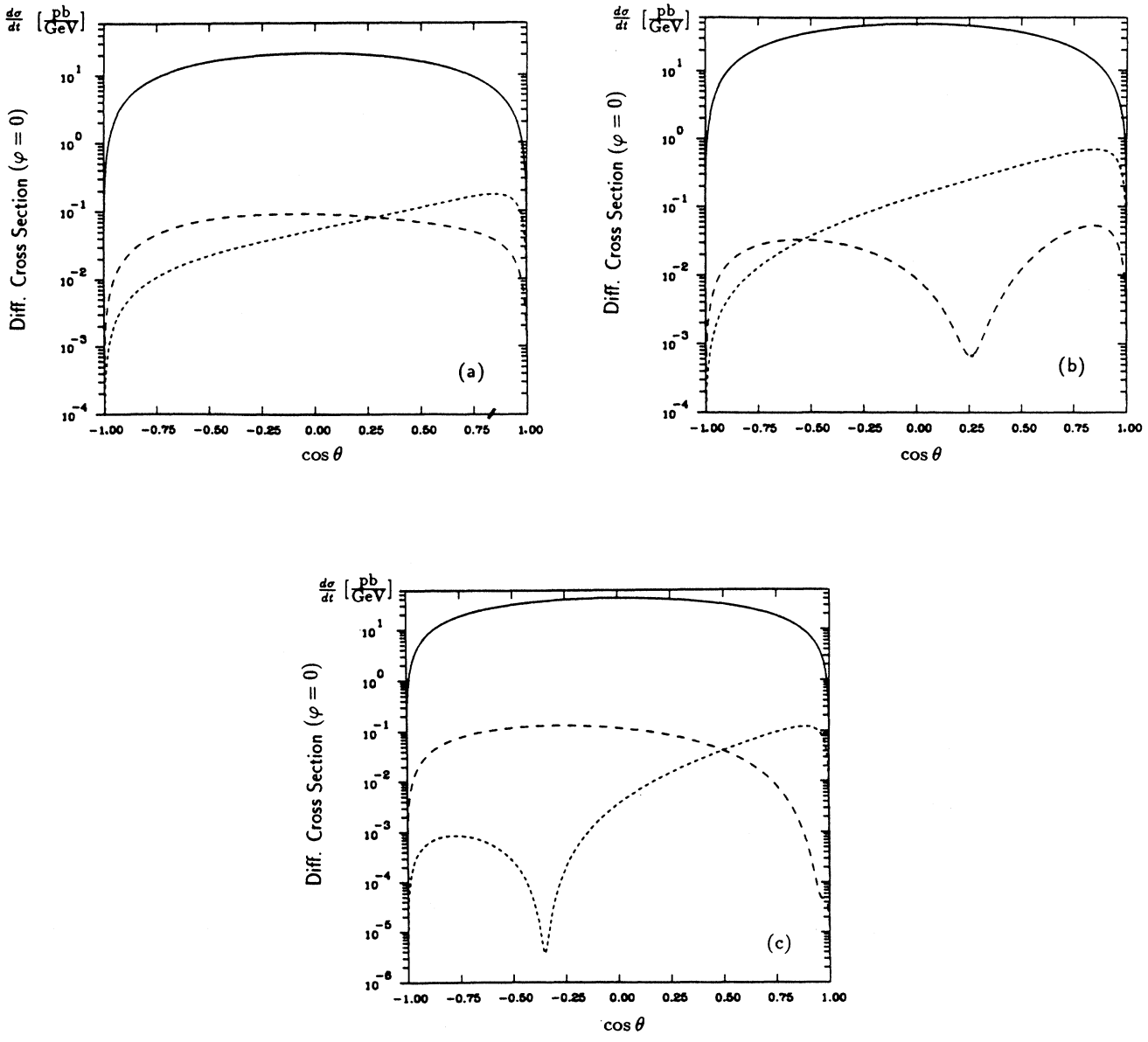

FIG. 3. Angular distributions of $e^-e^+\to\tilde{\nu}_e\bar{\tilde{\nu}}_e$ in scenario D for $M_{\tilde{\nu}_e}=40$ GeV and different beam polarizations ($\varphi=0$). (a) for unpolarized beams, (b) for longitudinal polarization (long$_{-+}$) and (c) for transverse polarization. Solid line denotes $\sqrt{s}=m_Z$, long-dashed line denotes $\sqrt{s}=120$ GeV, and short-dashed line denotes $\sqrt{s}=200$ GeV.

$$\frac{d\sigma}{dt}=\frac{e^4}{64\pi s_W^4}\frac{ut-M_{\tilde{\nu}}^4}{s^2}\left[(1+P_L)(1-P_L')\frac{s_W^4}{c_W^4}|D_z(s)|^2\right.$$
$$+(1-P_L)(1+P_L')\left[\frac{(c_W^2-s_W^2)^2}{4c_W^4}|D_z(s)|^2+\frac{c_W^2-s_W^2}{c_W^2}\left(\sum_j|V_{j1}|^2D_j(t)\right)\mathrm{Re}D_z(s)\right.$$
$$\left.+\left(\sum_j|V_{j1}|^2D_j(t)\right)^2\right]$$
$$+P_\perp P_\perp'\left\{\cos 2\varphi\left[\frac{s_W^2(c_W^2-s_W^2)}{c_W^4}|D_z(s)|^2+\frac{2s_W^2}{c_W^2}\left(\sum_j|V_{j1}|^2D_j(t)\right)\mathrm{Re}D_z(s)\right]\right.$$
$$\left.\left.-\sin 2\varphi\left[\frac{2s_W^2}{c_W^2}\left(\sum_j|V_{j1}|^2D_j(t)\right)\mathrm{Im}D_z(s)\right]\right\}\right]. \tag{2.6}$$

(The cross section for unpolarized beams obtained from Eq. (2.6) differs from the one given by Bartl *et al.* in Ref. [8]. The reason for this discrepancy is an error in Eq. (14) of Ref. [8].) Here P_L and $P_\perp$ are the longitudinal and transverse degrees of polarization of the electron, respectively, while P_L' and $P_\perp'$ are those of the positron. These quantities are defined in Eqs. (A3) and (A4) of the Appendix.

In the case of $\tilde{\nu}_\mu$ *and* $\tilde{\nu}_\tau$ *production,* only Z^0 exchange contributes. The corresponding cross sections are obtained from Eq. (2.6) by setting all chargino couplings to zero:

$$\frac{d\sigma}{dt}=\frac{e^4}{64\pi c_W^4}\frac{ut-M_{\tilde{\nu}}^4}{s^2}|D_z(s)|^2\left[(1+P_L)(1-P_L')+(1-P_L)(1+P_L')\frac{(c_W^2-s_W^2)^2}{4s_W^4}+P_\perp P_\perp'\cos 2\varphi\frac{c_W^2-s_W^2}{s_W^2}\right]. \tag{2.7}$$

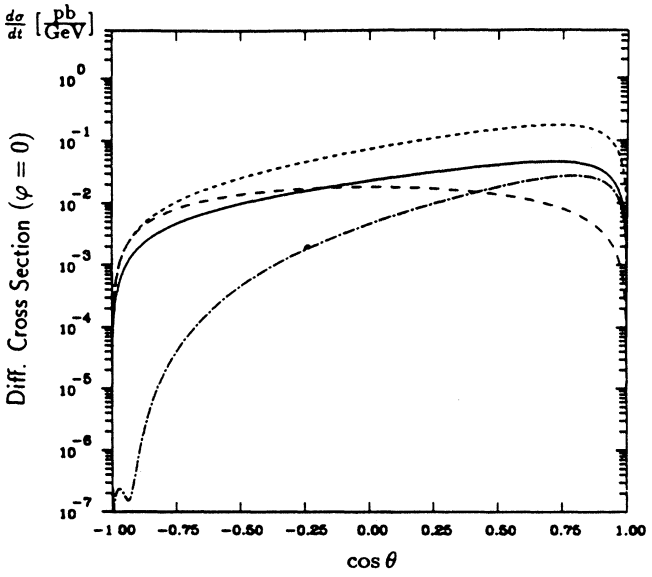

FIG. 4. Angular distributions of $e^-e^+\to\tilde{\nu}_e\bar{\tilde{\nu}}_e$ in scenario D for $M_{\tilde{\nu}_e}=80$ GeV and $\sqrt{s}=200$ GeV for different beam polarizations ($\varphi=0$). Solid line denotes unpolarized, short-dashed line denotes long$_{-+}$, long-dashed line denotes long$_{+-}$, and dashed-dotted line denotes transverse.

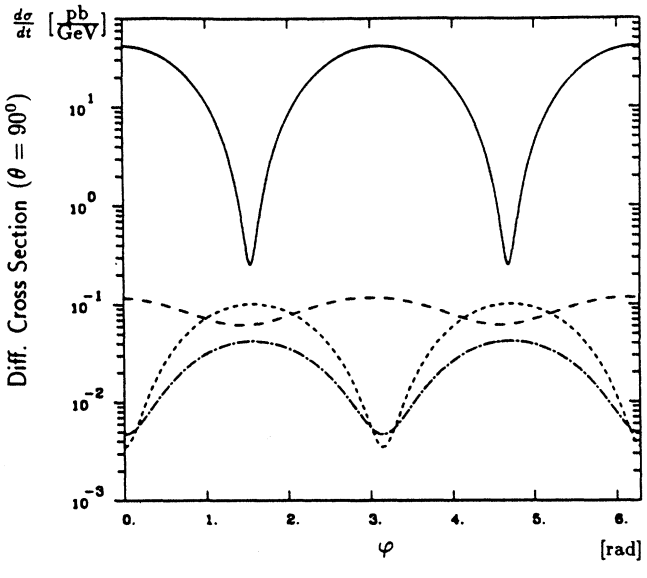

FIG. 5. Azimuth dependence of the differential cross section ($\theta=90°$) of $e^-e^+\to\tilde{\nu}_e\bar{\tilde{\nu}}_e$ for transversely polarized beams in scenario D. Solid line denotes $M_{\tilde{\nu}_e}=40$ GeV, $\sqrt{s}=m_z$, short-dashed line denotes $M_{\tilde{\nu}_e}=40$ GeV, $\sqrt{s}=200$ GeV, long-dashed line denotes $M_{\tilde{\nu}_e}=40$ GeV, $\sqrt{s}=120$ GeV, and dashed-dotted line denotes $M_{\tilde{\nu}_e}=80$ GeV, $\sqrt{s}=200$ GeV.

Obtaining analytical expressions for the total cross sections involves extensive algebra. Therefore, we have made use of a computer language (MACSYMA) allowing algebraic and calculus operations symbolically, i.e., for general, non-numerical expressions. The analytic integrations for the cross sections have been performed with a MACSYMA program on a Digital VAX mainframe at the Würzburg University Computing Center [9]. We obtain

$$\sigma_{\text{tot}}=(1+P_L)(1-P'_L)B_1+(1-P_L)(1+P'_L)B_2 \tag{2.8}$$

with

$$B_1=\frac{2\pi\alpha^2}{3c_W^4}\frac{Ep^3}{s}|D_z(s)|^2\,, \tag{2.9}$$

$$\begin{aligned}
B_2=&-f_c c_W^4 V_{21}^4 C_6\left[\frac{[2\ln(C_1-C_3)+1]C_3^2+[C_1-2C_1\ln(C_1-C_3)]C_3-C_1^2}{C_1^3C_3-C_1^4}\right.\\
&\left.-\frac{[2\ln(-C_3-C_1)+1]C_3^2+[2C_1\ln(-C_3-C_1)-C_1]C_3-C_1^2}{C_1^3C_3+C_1^4}\right]\\
&+f_c c_W^4 V_{21}^4 C_6\left[\frac{1}{C_1C_3-C_1^2}-\frac{1}{C_1C_3+C_1^2}\right]\\
&-2f_c c_W^4 V_{11}^2 V_{21}^2 C_6\left[\frac{\ln(C_1-C_3)C_3^2+C_1C_3-\ln(C_1-C_2)C_2^2-C_1C_2}{C_1^3C_3-C_1^3C_2}\right.\\
&\left.-\frac{\ln(-C_3-C_1)C_3^2-C_1C_3-\ln(-C_2-C_1)C_2^2+C_1C_2}{C_1^3C_3-C_1^3C_2}\right]\\
&+2f_c c_W^4 V_{11}^2 V_{21}^2 C_6\left[\frac{\ln(C_1-C_3)-\ln(C_1-C_2)}{C_1C_3-C_1C_2}-\frac{\ln(-C_1-C_3)-\ln(-C_1-C_2)}{C_1C_3-C_1C_2}\right]\\
&-V_{21}^2 C_4 C_6\left[\frac{2\ln(-C_3-C_1)C_3^2-2C_1C_3+C_1^2}{2C_1^3}-\frac{2\ln(C_1-C_3)C_3^2+2C_1C_3+C_1^2}{2C_1^3}\right]\\
&+V_{21}^2 C_4 C_6\left[\frac{\ln(-C_1-C_3)}{C_1}-\frac{\ln(C_1-C_3)}{C_1}\right]\\
&-f_c c_W^4 V_{11}^4 C_6\left[\frac{[2\ln(C_1-C_2)+1]C_2^2+[C_1-2C_1\ln(C_1-C_2)]C_2-C_1^2}{C_1^3C_2-C_1^4}\right.\\
&\left.-\frac{[2\ln(-C_1-C_2)+1]C_2^2+[-C_1+2C_1\ln(-C_1-C_2)]C_2-C_1^2}{C_1^3C_2+C_1^4}\right]\\
&+f_c c_W^4 C_6 V_{11}^4\left[\frac{1}{C_1C_2-C_1^2}-\frac{1}{C_1C_2+C_1^2}\right]\\
&-V_{11}^2 C_4 C_6\left[\frac{2\ln(-C_2-C_1)C_2^2-2C_1C_2+C_1^2}{2C_1^3}-\frac{2\ln(C_1-C_2)C_2^2+2C_1C_2+C_1^2}{2C_1^3}\right]\\
&+V_{11}^2 C_4 C_6\left[\frac{\ln(-C_1-C_2)}{C_1}-\frac{\ln(C_1-C_2)}{C_1}\right]+\frac{4}{3}C_5C_6\,.
\end{aligned} \tag{2.10}$$

In the above results, set $f_c=1$ for electron sneutrinos $\tilde{\nu}_e$ and $f_c=0$ for sneutrinos of other generations $(\tilde{\nu}_\mu,\tilde{\nu}_\tau)$. Furthermore, the following abbreviations have been used:

$$
\begin{aligned}
C_1&=\tfrac{1}{2}\sqrt{s-4m_e^2}\sqrt{s-4M_{\tilde{\nu}}^2}\ ,\\
C_3&=-\frac{s}{2}+M_{\tilde{\nu}}^2+m_e^2-m_1^2\ ,\\
C_3&=-\frac{s}{2}+M_{\tilde{\nu}}^2+m_e^2-m_2^2\ ,\\
C_4&=\frac{f_c c_W^2(2c_W^2-1)(s-m_Z^2)}{(s-m_Z^2)^2+\Gamma_Z^2 m_Z^2}\ ,\\
C_5&=\frac{(2c_W^2-1)^2}{4[(s-m_Z^2)^2+\Gamma_Z^2 m_Z^2]}\ ,\\
C_6&=\frac{\pi\alpha^2(s-4m_e^2)^{1/2}(s-4M_{\tilde{\nu}}^2)^{3/2}}{32c_W^4(c_W^2-1)^2 s}\ .
\end{aligned}
\tag{2.11}
$$

To provide a convincing consistency check, we have evaluated these expressions numerically and compared to the numerical integration (two-dimensional Romberg algorithm) of the differential cross section. In addition, we produced the results in another computer language (MATHEMATICA) on a PC. In both cases, the relative deviations were less than 10^{-6}.

The last paragraph of this section is dedicated to *polarization asymmetries.* For the *differential cross section,* we

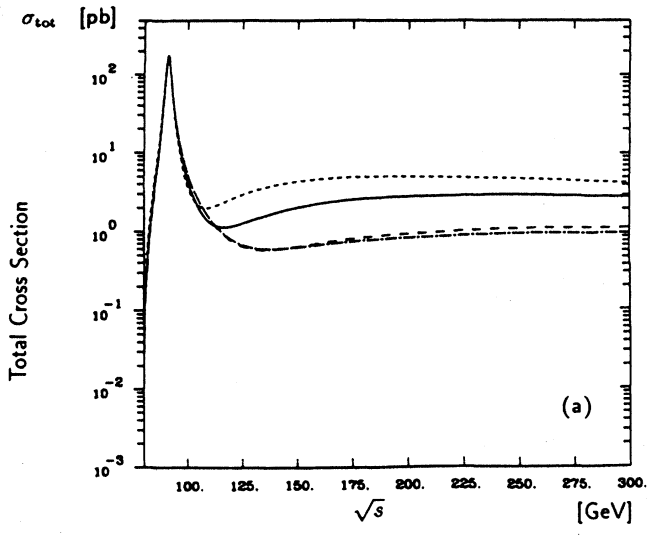

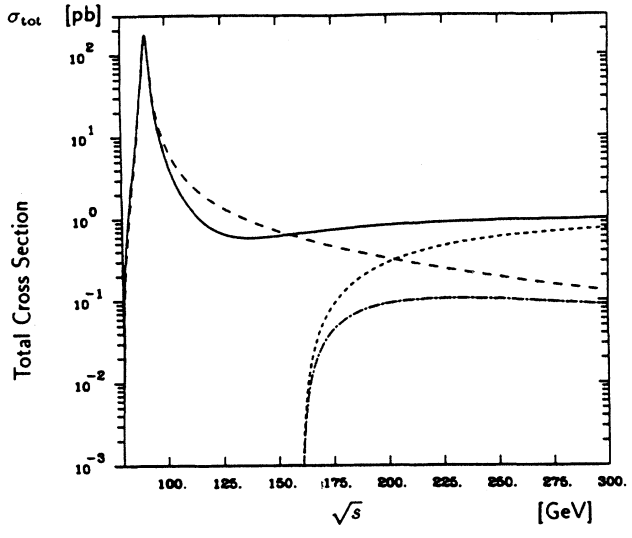

FIG. 6. Total cross section for the production of $\tilde{\nu}_e$ and $\tilde{\nu}_{\mu,\tau}$, respectively, with unpolarized beams in scenario D for different sneutrino masses. Solid line denotes $\tilde{\nu}_e(M_{\tilde{\nu}_e}=40$ GeV), short-dashed line denotes $\tilde{\nu}_e(M_{\tilde{\nu}_e}=80$ GeV), long-dashed line denotes $\tilde{\nu}_{\mu,\tau}(M_{\tilde{\nu}_{\mu,\tau}}=40$ GeV), and dashed-dotted line denotes $\tilde{\nu}_{\mu,\tau}(M_{\tilde{\nu}_{\mu,\tau}}=80$ GeV).

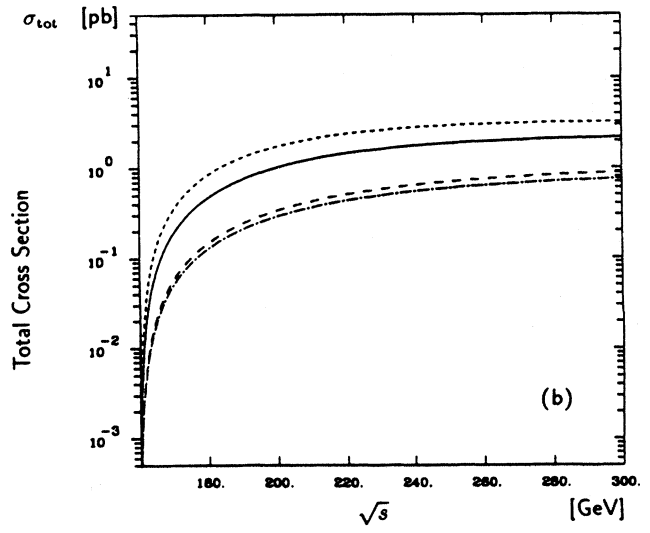

FIG. 7. Total cross section of $e^-e^+\to\tilde{\nu}_e\bar{\tilde{\nu}}_e$ with unpolarized beams in different chargino mixing scenarios. (a) for $M_{\tilde{\nu}_e}=40$ GeV, (b) for $M_{\tilde{\nu}_e}=80$ GeV. Solid line denotes scenario A, short-dashed line denotes scenario C, long-dashed line denotes scenario B, and dashed-dotted line denotes scenario D.

define longitudinal-polarization asymmetries as

$$a_L(P_L,P_L'):=\frac{\frac{d\sigma}{dt}(P_L,P_L')-\frac{d\sigma}{dt}(-P_L,-P_L')}{\frac{d\sigma}{dt}(P_L,P_L')+\frac{d\sigma}{dt}(-P_L,-P_L')} \tag{2.12}$$

For one or both beams longitudinally polarized, we obtain

$$\begin{aligned} a_L &\equiv a_L(P_L=1,P_L'=-1)=a_L(P_L=1,P_L'=0) \\ &=-a_L(P_L=0,P_L'=1) \\ &=\frac{|F_{+1/2-1/2}|^2-|F_{-1/2+1/2}|^2}{|F_{+1/2-1/2}|^2+|F_{-1/2+1/2}|^2}\ . \end{aligned} \tag{2.13}$$

All other longitudinal-polarization asymmetries vanish. For the case of transverse (natural) polarization, we compare the cross sections for zero and nonzero polarization:

$$a_\perp(P_\perp,P_\perp')=\frac{d\sigma/dt(P_\perp,P_\perp')-d\sigma/dt(0,0)}{d\sigma/dt(P_\perp,P_\perp')+d\sigma/dt(0,0)}\ . \tag{2.14}$$

The only nonvanishing transverse-polarization asymmetry is

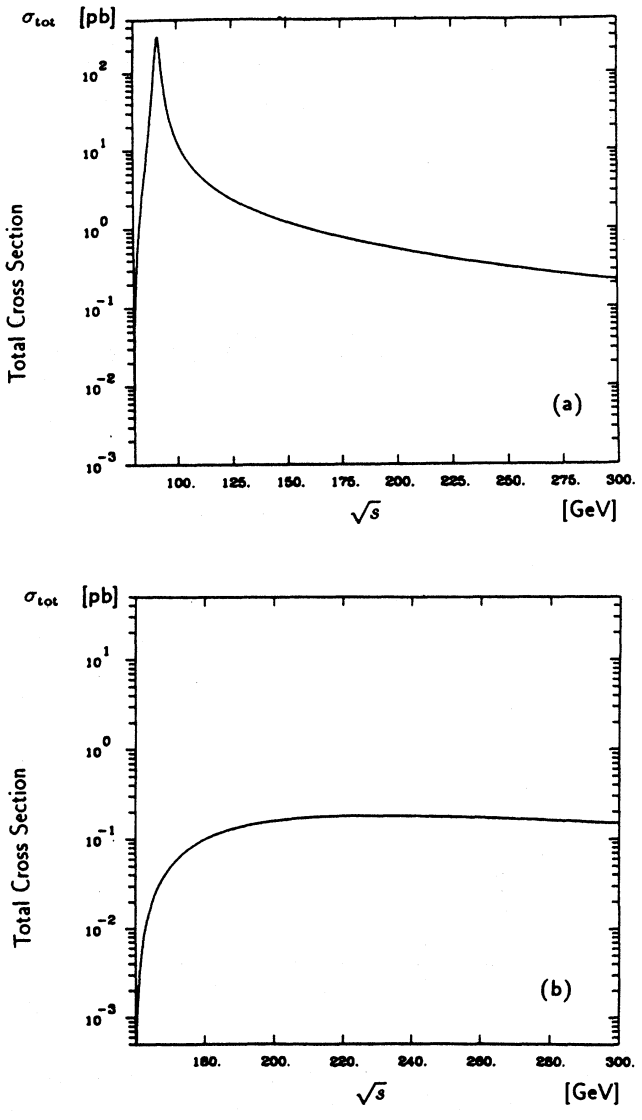

FIG. 8. Total cross section of $e^-e^+\to\tilde{\nu}_e\bar{\tilde{\nu}}_e$ for longitudinal polarization (long$_{+-}$), identical for all mixing scenarios. (a) for $M_{\tilde{\nu}_e}=40$ GeV, (b) for $M_{\tilde{\nu}_e}=80$ GeV.

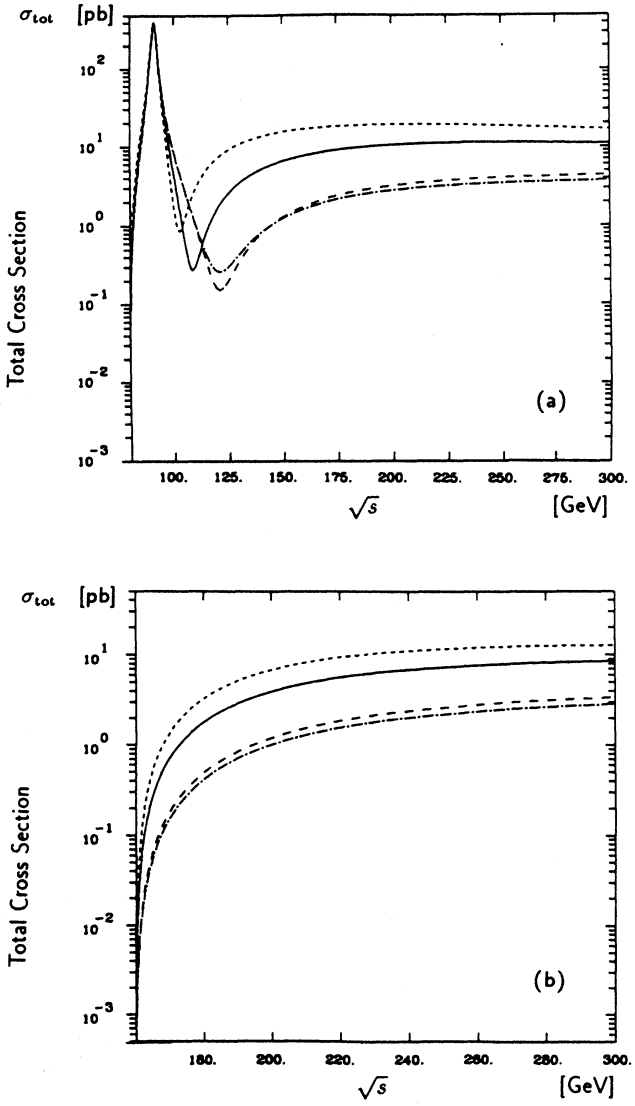

FIG. 9. Total cross section of $e^-e^+\to\tilde{\nu}_e\bar{\tilde{\nu}}_e$ for longitudinal polarization (long$_{-+}$) in different chargino mixing scenarios. (a) for $M_{\tilde{\nu}_e}=40$ GeV, (b) for $M_{\tilde{\nu}_e}=80$ GeV. Solid line denotes scenario A, short-dashed line denotes scenario C, long-dashed line denotes scenario B, and dashed-dotted line denotes scenario D.

$$a_\perp \equiv a_\perp(P_\perp=1,P'_\perp=1) = \frac{\mathrm{Re}(F_{-1/2+1/2}F^*_{+1/2-1/2})}{|F_{+1/2-1/2}|^2+|F_{-1/2+1/2}|^2+\mathrm{Re}(F_{-1/2+1/2}F^*_{+1/2-1/2})} . \quad (2.15)$$

For transversely polarized beams, all asymmetries of the *total cross sections* vanish. The nonvanishing longitudinal-polarization asymmetries of the total cross section

$$A_L(P_L,P'_L)=\frac{\sigma_{\mathrm{tot}}(P_L,P'_L)-\sigma_{\mathrm{tot}}(-P_L,-P'_L)}{\sigma_{\mathrm{tot}}(P_L,P'_L)+\sigma_{\mathrm{tot}}(-P_L-P'_L)} \quad (2.16)$$

satisfy a relation completely analogous to Eq. (2.13):

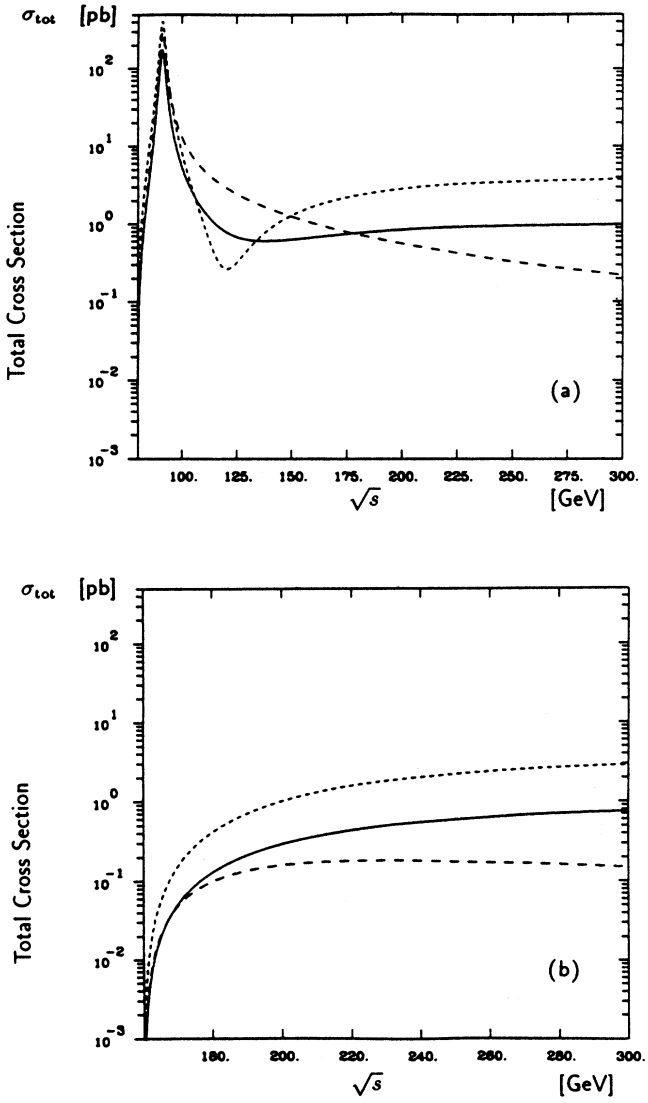

FIG. 10. Total cross section of $e^-e^+\to\tilde{\nu}_e\bar{\tilde{\nu}}_e$ in scenario D for different beam polarizations. (a) for $M_{\tilde{\nu}_e}=40$ GeV, (b) for $M_{\tilde{\nu}_e}=80$ GeV. Solid line denotes unpolarized (transverse), long-dashed line denotes long$_{+-}$, and short-dashed line denotes long$_{-+}$.

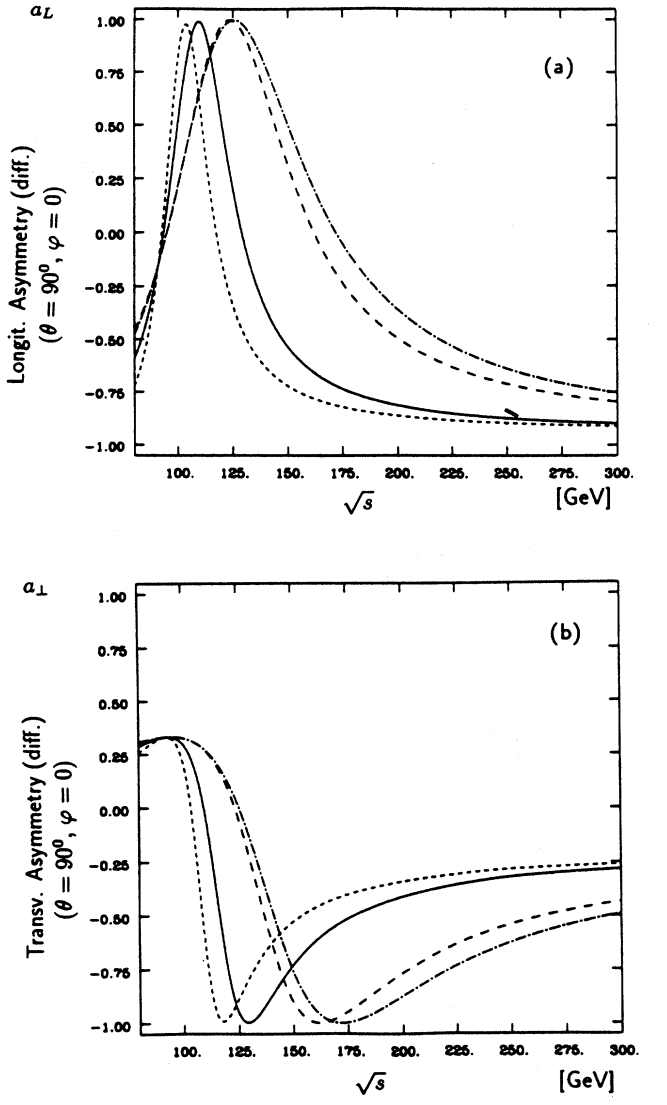

FIG. 11. Polarization asymmetries of the *differential* cross section ($\theta=90°$, $\varphi=0$) of $e^-e^+\to\tilde{\nu}_e\bar{\tilde{\nu}}_e$ for different chargino mixing scenarios and $M_{\tilde{\nu}_e}=40$ GeV. (a) for longitudinal polarization, (b) for transverse polarization. Solid line denotes scenario A, short-dashed line denotes scenario C, long-dashed line denotes scenario B, and dashed-dotted line denotes scenario D.

$$A_L \equiv A_L(P_L=1,P_L'=-1)=A_L(P_L=1,P_L'=0)$$
$$=-A_L(P_L=0,P_L'=1)\ . \qquad (2.17)$$

III. NUMERICAL RESULTS AND DISCUSSION

To illustrate the influence of chargino mixing on cross sections and polarization asymmetries, we shall present numerical results for four different scenarios.

The masses and also the couplings of the charginos being determined by the parameters of the W-ino–charged-Higgsino mass matrix (see Refs. [10] and [7] for details) are strongly model dependent. From an analysis of the Z^0 decay properties, the L3 Collaboration [11] obtained a lower bound of 44 GeV for the chargino mass, assuming the lighter chargino to be a pure W-ino, while the ALEPH Collaboration [12] gave a lower limit of 45.5 GeV for this case and 44.5 GeV for a pure Higgsino.

We have adjusted the parameters of the mass matrix such that all our scenarios are compatible with the most stringent chargino mass bounds given above. The main differences between the four scenarios are the nature and

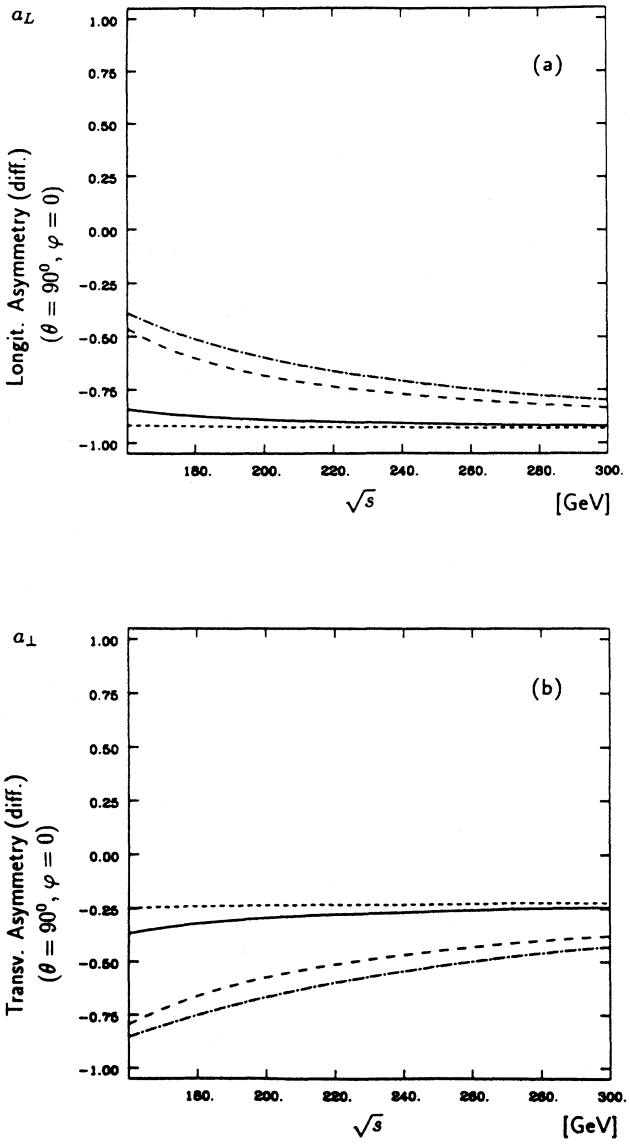

FIG. 12. The same as Fig. 11 for $M_{\tilde{\nu}_e}=80$ GeV.

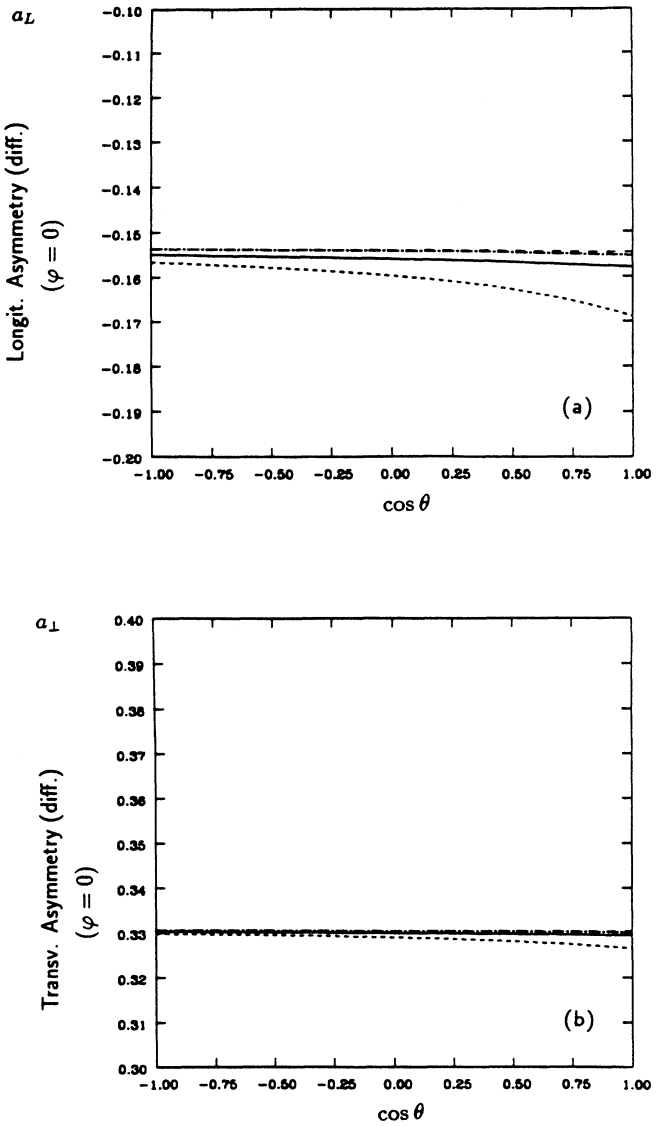

FIG. 13. Angular distribution of the polarization asymmetries for $e^-e^+\to\tilde{\nu}_e\bar{\tilde{\nu}}_e$ in different chargino mixing scenarios ($\varphi=0$) for $M_{\tilde{\nu}_e}=40$ GeV and $\sqrt{s}=m_z$. (a) for longitudinal polarization, (b) for transverse polarization. Solid line denotes scenario A, short-dashed line denotes scenario C, long-dashed line denotes scenario B, and dashed-dotted line denotes scenario D.

the mass of the light chargino $\tilde{\chi}_2^+$: It is predominantly W-ino in scenarios A and C, predominantly Higgsino in scenarios B and D (refer to Table I for scenario parameters); its mass is relatively large (roughly 76 GeV) in scenarios A and B, comparatively small (about 55 GeV) in C and D. In order to see the influence of the sneutrino mass, we have also distinguished the case of a light ($M_{\tilde{\nu}}=40$ GeV) or a heavy ($M_{\tilde{\nu}}=80$ GeV) sneutrino.

The eight configurations we can choose from will be denoted as AL (scenario A, light sneutrino) through DH (scenario D, heavy sneutrino). We will also refer to four special cases of polarization: unpolarized ($\mathbf{P}=\mathbf{P}'=0$), long$_{+-}$($P_L=1, P'_L=-1$), long$_{-+}$($P_L=-1, P'_L=1$), and transverse($P_\perp=P'_\perp=1$). As can be seen from Eqs. (2.6) and (2.7), cross sections vanish for two longitudinally polarized beams of equal helicities ($P_L=P'_L=\pm 1$). Since only Z^0 exchange contributes to the configuration long$_{+-}$, comparison of the cases long$_{+-}$ and long$_{-+}$ should allow conclusions on chargino mixing. For the Z^0 mass and decay width we have used the values $m_Z=91.1\pm0.053$ GeV and $\Gamma_Z=2.59\pm0.075$ GeV found, e.g., in Refs. [13]–[16].

Let us now give some comments on our numerical results. The strong variation with polarization displayed by the *differential cross section* for electron sneutrinos $\tilde{\nu}_e$ is demonstrated in Fig. 2 for scenario D. For the case of light sneutrinos ($M_{\tilde{\nu}} \lesssim m_Z/2$) up to $\sqrt{s} \approx 100$ GeV Z^0 exchange dominates by far, suppressing the dependence on polarization and also the effect of chargino mixing. In the region between 100 and 200 GeV, however, considerable interference effects between s- and t-channel exchange give rise to cross sections differing by several orders of magnitude for different polarization configurations. If, in turn, the sneutrino mass is consid-

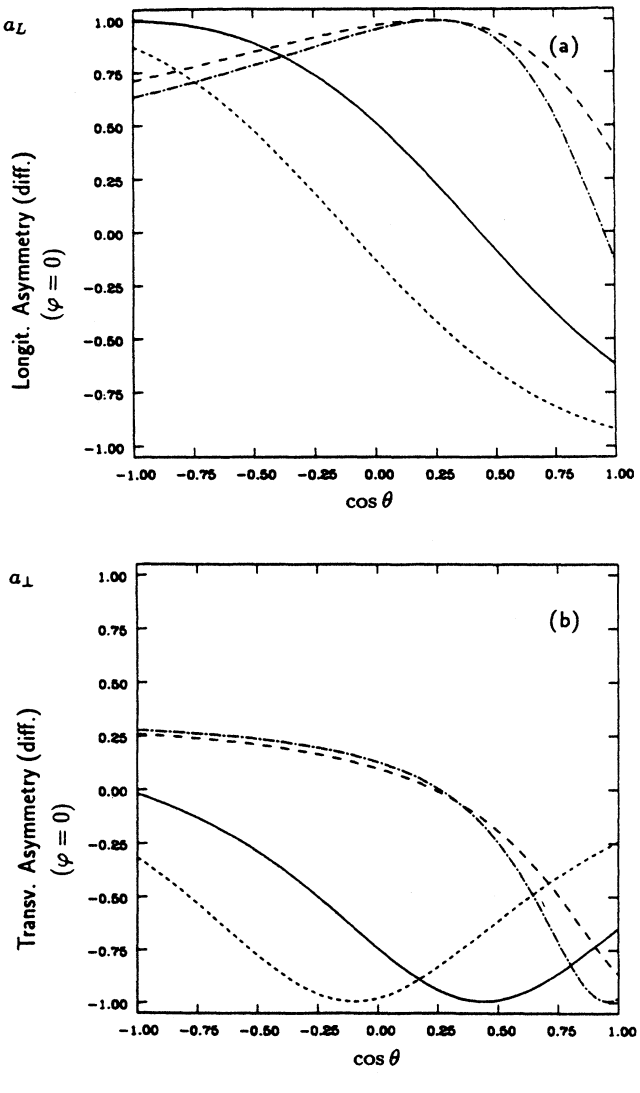

FIG. 14. The same as Fig. 13 for $M_{\tilde{\nu}_e}=40$ GeV and $\sqrt{s}=120$ GeV.

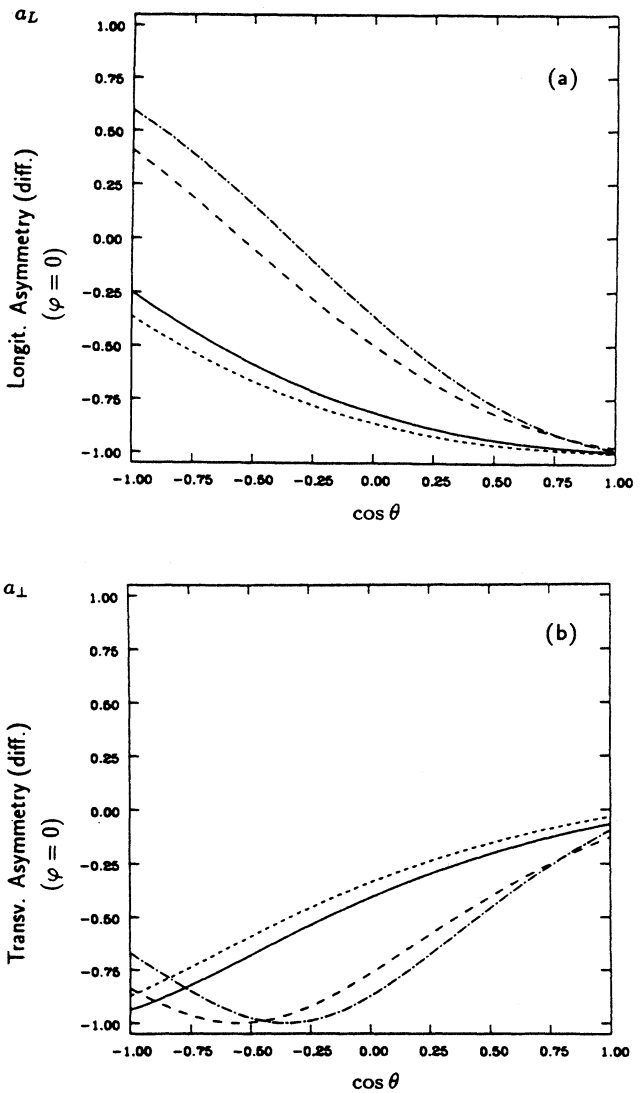

FIG. 15. The same as Fig. 13 for $M_{\tilde{\nu}_e}=40$ GeV and $\sqrt{s}=200$ GeV.

erably larger than $m_Z/2$, apart from the rapid increase in the threshold region one obtains flat cross sections without any structure. All cross sections—except that for polarization long_{+-} allowing only Z^0 exchange—are still slowly increasing in the region from about 190 to 300 GeV.

Figures 3(a) to 3(c) show for the light-sneutrino case angular distributions for different energies ($\sqrt{s}=m_Z$, 120 GeV, 200 GeV) and polarization configurations. While for $\sqrt{s}=m_Z$, Z^0 dominance causes a strict $\sin^2\theta$ dependence, with increasing energy the asymmetric contribution of chargino exchange creates interesting structures. For the case of a heavy sneutrino (Fig. 4) we give angular distributions for $\sqrt{s}=200$ GeV only, where Z^0 exchange is already strongly suppressed.

For transversely polarized beams, the differential cross section displays a more or less intensive, periodic variation with the azimuth φ (Fig. 5), the phase being shifted by π between energies of 120 and 200 GeV. We have not shown the long_{+-} polarization case, since it only allows the s-channel process and thus never deviates from perfect symmetry for whatever energy.

We have not explicitly given angular distributions for $\tilde{\nu}_{\mu,\tau}$ production since it is completely analogous to the $\sin^2\theta$ distribution for $\tilde{\nu}_e$ production with polarization long_{+-}.

We continue with the discussion of the *total cross sections*. Figure 6 shows total cross sections (in scenarios DL and DH) for unpolarized beams, comparing the pro-

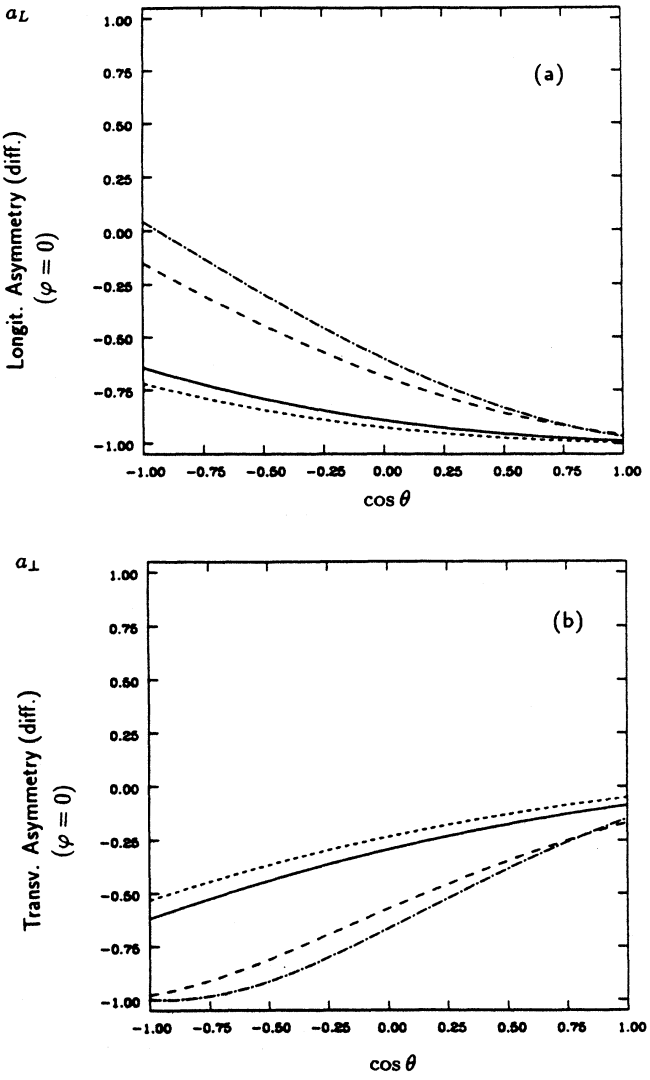

FIG. 16. The same as Fig. 13 for $M_{\tilde{\nu}_e}=80$ GeV and $\sqrt{s}=200$ GeV.

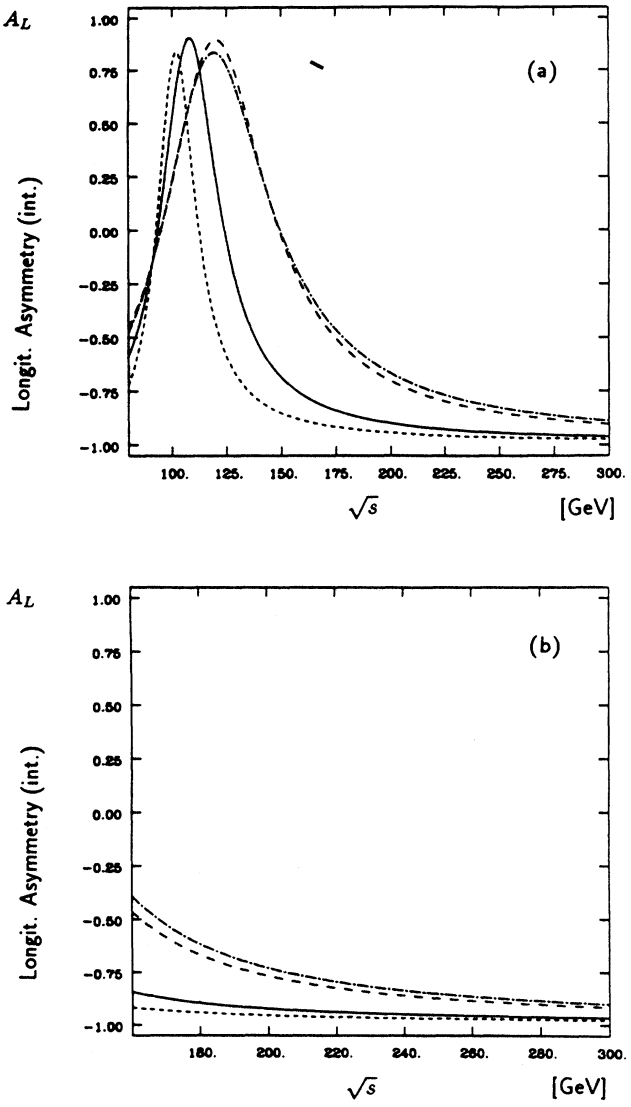

FIG. 17. (Longitudinal) polarization asymmetry of the *total* cross section for the process $e^-e^+\to\tilde{\nu}_e\bar{\tilde{\nu}}_e$ for different chargino mixing scenarios. (a) for $M_{\tilde{\nu}_e}=40$ GeV, (b) for $M_{\tilde{\nu}_e}=80$ GeV. Solid line denotes scenario A, short-dashed line denotes scenario C, long-dashed line denotes scenario B, and dashed-dotted line denotes scenario D.

duction of electron sneutrinos, on one hand, μ or τ sneutrinos, on the other hand. In the second case, chargino exchange is absent. As one would expect, the contribution of Z^0 exchange decreases rapidly with increasing distance from the peak, whereas the chargino process keeps rising for quite a while. Thus, for example, at 200 GeV, electron sneutrinos may be produced at a rate more than ten times higher than that for $\tilde{\nu}_\mu$ or $\tilde{\nu}_\tau$, leaving some hope for LEP II.

Figure 7 through 9 illustrate the influence of chargino mixing and sneutrino mass on the total cross sections. For unpolarized beams and polarization long$_{-+}$, varying chargino mixing creates changes of up to one or two orders of magnitude at energies above the Z^0 pole, decreasing for higher energies. For polarization long$_{+-}$, chargino exchange is prohibited and the cross sections are the same for all scenarios.

To facilitate comparisons, we have grouped the total cross sections for all polarizations and scenario D in one picture. For light sneutrino in Fig. 10(a), for heavy sneutrino in Fig. 10(b). At high energies between 200 and 300 GeV, the cross sections vary by up to one order of magnitude for different polarizations, while the influence of chargino mixing is reduced to about a factor of 2.

The last group of graphs is dedicated to the polarization asymmetries of the differential and of the total cross sections. In Figs. 11 and 12, we show the energy dependence of longitudinal and transverse asymmetries of the differential cross section. We find large asymmetries strongly varying with energy. Especially for the case of a light sneutrino, the longitudinal asymmetry runs all the way from $+1$ to -1. Chargino mixing gives rise to quantitative effects without changing the qualitative behavior.

There is also a general observation one can make: As far as absolute values are concerned, transverse asymmetry is large where the longitudinal one is small, and vice versa. A similar fact is well known in the production of nonsupersymmetric particles, except than in those cases longitudinal asymmetries carry the same, but transverse asymmetries opposite sign [2]. This might be one more feature facilitating the task to distinguish the production of supersymmetric particles from background events.

The variation of (longitudinal and transverse) differential asymmetries with the scattering angle θ are studied in Figs. 13 to 16: With light sneutrinos for energies of 91.1 GeV ($=m_Z$), 120 and 200 GeV, heavy sneutrinos for 200 GeV only. Please note the extremely magnified scale in Fig. 13—both asymmetries are practically constant and independent of chargino mixing, in agreement with our general remarks about the "boring" behavior of just about any quantity at the Z^0 peak.

This changes a lot for higher energies: Now chargino exchange dominates and confirms our expectation of strong variations with mixing scenarios. The chiral structure of couplings causes large asymmetries of the cross section.

We conclude with the longitudinal asymmetry of total cross sections, shown in Figs. 17(a) and 17(b) for light and heavy scenarios, respectively, versus energy. See also Figs. 11(a) and 12(a) for comparison: Like the longitudinal asymmetry of differential cross sections depicted there, this one depends very much on c.m.-system energy, somewhat on chargino mixing and approaches the value -1 for high energies.

ACKNOWLEDGMENTS

One of us (M.W.) would like to thank J. Küblbeck and R. Mertig [9] for their valuable advice. Their assistance in generating computer algebra programs contributed very much to the facilitation of our calculations. M.W. was supported in part by "Studienstiftung des Deutschen Volkes", D-5300 Bonn, F.R.G. H.F. was supported by "Bundesministerium für Forschung und Technologie" (BMFT), D-5300 Bonn, F.R.G., Förderungskennzeichen 055WU91P2.

APPENDIX

We give a brief summary of our notations and conventions for the description of beam polarization. For details we refer the reader to Ref. [17].

Laboratory and center-of-mass systems being identical, we choose coordinates such that the four-momenta of electrons and positrons read

$$l^\mu=(l^0,\boldsymbol{l})=(l^0,0,0,l)$$

and (A1)

$$l'^\mu=(l^0,-\boldsymbol{l})=(l^0,0,0,-l)\ ,$$

respectively, with $l=|\boldsymbol{l}|$ and $E=l^0=\sqrt{l^2+m_e^2}\approx l$. Momentum conservation requires $\mathbf{p}'=-\mathbf{p}$ for the (anti)sneutrino momenta, where the $\tilde{\nu}$ four-momentum is given by $p^\mu=(p^0,p\sin\theta\cos\varphi,p\sin\theta\sin\varphi,p\cos\theta)$.

For the electron, the Lorentz-covariant polarization vector ξ^μ and the three-dimensional, spatial polarization vector $\mathbf{P}=(P^1,P^2,P^3)$ of the electron beam are connected via

$$\xi^\mu=\left(P^3\frac{l}{m_e},P^1,P^2,P^3\frac{l^0}{m_e}\right)\ . \tag{A2}$$

In the case of a longitudinally polarized beam, we have $\mathbf{P}=(0,0,P_L)$, whereas $\mathbf{P}=(P^1,P^2,0)=\mathbf{P}_\perp$ for transverse beam polarization.

In the helicity basis, the spin-density matrix of the electrons takes the explicit form

$$\rho_{\lambda_1\lambda_2}=\frac{1}{2}\begin{pmatrix}1+P_L & P_1-iP_2\\ P_1+iP_2 & 1-P_L\end{pmatrix}=\frac{1}{2}\begin{pmatrix}1+P_L & P_\perp e^{-i\beta}\\ P_\perp e^{i\beta} & 1-P_L\end{pmatrix}\ , \tag{A3}$$

where $\lambda_{1,2}=\pm\frac{1}{2}$. The polarization vector $\mathbf{P}'$ of the positron beam and the positron spin-density matrix

$$\rho'_{\lambda'_1\lambda'_2}=\frac{1}{2}\begin{bmatrix}1+P'_L & P'_1-iP'_2\\ P'_1+iP'_2 & 1-P'_L\end{bmatrix}$$
$$=\frac{1}{2}\begin{bmatrix}1+P'_L & P'_\perp e^{-i\beta}\\ P'_\perp e^{i\beta} & 1-P'_L\end{bmatrix} \quad \text{(A4)}$$

are defined similarly to the electron case (see Ref. [17] for phase conventions). To obtain the last form of ρ and ρ', we have fixed the x axis such that it bisects the angle 2β spanned by $\mathbf{P}$ and $\mathbf{P}'$. Hence the y axis points in the direction of the "natural" polarization of the electron beam (i.e., perpendicular to the plane of the electron orbits and antiparallel to the magnetic field).

From the spin-density matrices and the helicity amplitudes $F_{\lambda\lambda'}$, the transition probability is calculated according to

$$|\mathcal{T}_{fi}|^2=\sum_{\substack{\lambda_1,\lambda_2\\ \lambda'_1,\lambda'_2}}\rho_{\lambda_1\lambda_2}\rho'_{\lambda'_1\lambda'_2}F_{\lambda_1\lambda'_1}F^*_{\lambda_2\lambda'_2}\ . \quad \text{(A5)}$$

For our special process with $F_{+1/2,+1/2}=F_{-1/2-1/2}=0$, we find

$$|\mathcal{T}_{fi}|^2=\frac{1}{4}[\,(1+P_L)(1-P'_L)|F_{+1/2-1/2}|^2$$
$$+(1-P_L)(1+P'_L)|F_{-1/2+1/2}|^2$$
$$+2P_\perp P'_\perp \mathrm{Re}(F_{-1/2+1/2}F^*_{+1/2-1/2})] \quad \text{(A6)}$$

independent of the angle 2β between $\mathbf{P}$ and $\mathbf{P}'$.

[1] OPAL Collaboration, M. Akrawy *et al.*, Phys. Lett. B **248**, 211 (1990).
[2] P. Chiappetta, *et al.*, Nucl. Phys. **B259**, 365 (1985).
[3] *Physics at LEP,* LEP Jamboree, Geneva, Switzerland, 1985, edited by J. Ellis and R. Peccei (CERN Yellow Report No. 86-02, Geneva, 1986), Vol. 1.
[4] H. E. Haber, R. M. Barnett, and K. S. Lackner, Phys. Rev. D **29**, 1990 (1984).
[5] R. M. Barnett, H. E. Haber, and K. S. Lackner, Phys. Rev. D **29**, 1381 (1984).
[6] H. E. Haber and G. L. Kane, Phys. Rep. **117**, 75 (1985).
[7] A. Bartl, H. Fraas, and W. Majerotto, Z. Phys. C **30**, 441 (1986); Nucl. Phys. **B278**, 1 (1986).
[8] A. Bartl, H. Fraas, and W. Majerotto, Z. Phys. C **34**, 411 (1987).
[9] J. Küblbeck and R. Mertig, University of Würzburg, Federal Republic of Germany, private communication.
[10] H. E. Haber and G. L. Kane, Phys. Rep. **117**, 219ff (1985).
[11] L3 Collaboration, B. Adeva *et al.*, Phys. Lett. B **233**, 530 (1989).
[12] ALEPH Collaboration, D. Decamp *et al.*, Phys. Lett. B **236**, 86 (1990).
[13] L3 Collaboration, B. Adeva *et al.*, Phys. Lett. B **231**, 509 (1989).
[14] ALEPH Collaboration, D. Decamp *et al.*, Phys. Lett. B **231**, 519 (1989).
[15] OPAL Collaboration, M. Akrawy *et al.*, Phys. Lett. B **231**, 530 (1989).
[16] DELPHI Collaboration, P. Aarnio *et al.*, Phys. Lett. B **231**, 539 (1989).
[17] F. M. Renard, *Basics of Electron Positron Collisions* (Editions Frontières, Dreux, France, 1981).